HEAT TRANSFER ENHANCEMENT IN ROTATING DISK BOUNDARY-LAYER

by

Ahmer MEHMOOD and Muhammad USMAN*

Department of Mathematics and Statistics, FBAS, International Islamic University, Islamabad, Pakistan

Original scientific paper
https://doi.org/10.2298/TSCI160412293M

A generally admitted fact about the nanofluids is the expedition of heat transfer process in comparison to pure fluids. The calculation of enhanced rate of heat transfer depends strongly upon the nanofluid modeling. Following the experimental evidence most of the researchers assume the nanofluid to be a homogeneous mixture. However, this is a severe condition that results in under-prediction of heat transfer rates. Due to the ongoing convection phenomena the nanoparticle concentration is actually non-homogeneous within the boundary-layer because of the presence of concentration gradients. The objective of this study is to calculate the heat transfer enhancement in 3-D boundary-layer when the working fluid is a nanofluid. The rotating disk geometry, which perhaps serves as the bench mark for the 3-D boundary-layers, have been chosen for the purpose here. The non-homogeneous nanofluid modeling has been utilized and a percent increase in Nusselt number has been calculated. Detailed analyses of flow and heat transfer phenomena for nanofluids have been conducted under the influence of several physical parameters.

Key words: *nanofluid, rotating disk, heat transfer enhancement, non-homogeneous model*

Introduction

Heat and mass transfer phenomena occur in diverse engineering applications like heat and mass exchangers, computer storage devices, fluid flow, and convective heat transfer in rotor-stator systems (the rotor for a rotating disk and the stator for a stationary disk) are of great importance in turbomachinery and power engineering. Such situations require efficient heat transfer mechanism so that the working machinery can continue without any collapse. Therefore the engineers and scientist are always interested in searching for situations in which higher rates of heat transfer can be achieved. Different techniques are adopted, depending upon the suitability to the situation, in order to enhance the heat transfer process. Among many choices, one of the modern technique is the selection of nanofluid as a cooling agent. The notion of nanofluids comes from the fact that metals have higher thermal conductivity than liquids. Due to the advent of nanotechnology it became possible to create metallic particles of nanoscale size that can be mixed in a fluid (called base fluid) to form a nanofluid with enhanced thermal conductivity. Addition of small metallic particles has a big impact on thermophysical properties of the fluid. The flow and heat transfer with microsize particles was first studied by Maxwell

* Corresponding author, e-mail: usman725.iiui@gmail.com

[1] in 1904. Though he revealed some enhancement in heat transfer but the particle dimensions caused sedimentation, abrasion and clogging [2]. In order to keep the mixture homogeneous, the size of the particles needed to be minimized. This can now easily be achieved with the help of modern nanotechnology, which can produce particles of the size between 1-100 nm. Due to extremely small-sized particles, comparable to the size of the molecules of the base fluid, they are easily accommodated by the fluid and the aforementioned issues caused by the metallic particles get resolved. Choi [3] was the first who introduced the word 'nanofluid' for such fluids. In most of the available literature on nanofluids, the researchers modeled the nanofluid as a homogeneous mixture by incorporating the role of thermophoressis and Brownian motion [4, 5]. Several authors investigated heat and mass transfer phenomena through Buongiorno [4] and Tiwari and Das [5] models for variety of flow geometries, a few of them are mentioned here [6-9]. Based on this modeling Magia *et al.* [8] and Avramenko *et al.* [10, 11] pointed out that, due to homogeneous models, the heat transfer coefficients of nanofluid are underpredicted. The reason is the incorrect incorporating of local concentration of the nanoparticles within the boundary-layer. The drawback with the Buongiorno [4] and Tiwari and Das [5] models is the consideration of uniform distribution of nanoparticles in the base fluid. This is actually done on the basis of experimental evidence. However, the homogeneous distribution of nanoparticles is not sustained within the boundary-layer due to the relative motion of nanoparticles and fluid. Frank *et al.* [12] and Ding and Wen [13] theoretically proved the non-homogeneous distribution of nanoparticles in the nanofluid as a consequence of velocity and temperature gradients. The existence of concentration gradients is also confirmed through experiments [9]. Such a consideration also results in heat and mass transfer rate augmentation. This issue has recently been addressed by Avramenko *et al.* [10] where they successfully incorporated the effects of convective transport of nanoparticles on momentum, thermal and mass transfer phenomena within the boundary-layer. For detailed information it is fruitful to follow [14-16].

Rotating flow phenomena occur in diverse engineering applications, namely, turbines of rocket, gas turbines and centrifugal pumps, *etc.* These important applications in the leading areas of science and engineering motivate one to investigate heat and mass transfer phenomena in rotating boundary-layers. Rotating disk systems can be used to model the flow characteristics, together with heat and mass transfer rates, that arise in practical turbomachinery for instance the flow of waxy crude oils or foodstuffs in centrifugal pumps, air craft engines, car brake systems, computer disk drivers and electrochemistry [17]. There are different reasons for choosing the rotating disk system as a prototype for practical rotating flows. In order to search a preferable system to study the transport phenomena of fluid flow in 3-D boundary-layers, the rotating disk is confirmed to be the best choice. It allows the complete 3-D self-similar exact solution whereby reducing the coupled system of Navier-Stokes equations to a simple non-linear system of ODE. Despite the mentioning of above closely related engineering applications and the potential of mathematical simplification the rotating disk flow serves as the global paradigm for many 3-D flows, such as the flow on swept wings. The generation of spiral vortices at the edge of swept wings is similar in nature to the class of flow vortices developed due to the rotation of the disk in an infinite ambient fluid. The presence of the point of inflection in the laminar velocity curve of the rotating disk flow indicates the vulnerability of it to the cross-flow instability. This ultimately makes the rotating disk model as an alternative laboratory towards the study and understanding of many boundary-layer features associated particularly to the 3-D flows. Based on these observations and great resemblances among the rotating disk boundary-layer and the 3-D boundary-layer Lingwood [18] preferred to choose the rotating disk model towards the study of absolute instability associated to the 3-D flow. Her investigation concludes that

neither the Coriolis force nor the streamline curvature affect the absolute instability in the disk flow which confirms the application of the disk results to the swept wing case where the Coriolis effects are absent at all. Continuing with the Lingwood's choice of disk model Pier [19] proposed a new method in order to delay the onset of transition. This was accomplished by introducing a continuously supplied periodic force to the unstable region in order to improve the ongoing self-sustained non-linear dynamics. The laminar-turbulent transition in the boundary-layer flows can also be delayed, in some cases, because of the advantageous effects of the compliant walls. In order to investigate the supportive role of compliant wall in general, and to understand the drag reduction on the swimming dolphin's body due to the flexible nature of its skin in particular, Carpenter and Thomas [20] also preferred to choose the rotating disk model as the convenient flow geometry. Following the same analogy between the disk flow and 3-D boundary-layers, as utilized by the above researchers, Davies and Carpenter [21] also considered it as a proto type model of for the investigation of linear global behavior of the absolute instability in 3-D boundary-layers. Continuing in this way Imayama [22] contributed sufficient efforts towards the further understanding of the laminar-turbulent transition in the rotating disk flow. Further relevant, and of course interesting, studies can also be found in the bibliographic items of [22]. The general reason behind the preference to the rotating disk model in the above mentioned studies is the most general nature of disk flow that resembles in large to the 3-D flows. The glimpses from the bulk of available literature seem to be sufficient for the reader in order to make him realize the wider scope and physical richness of the von Karman swirling flow. Keeping this fact in mind the rotating disk flow has also been chosen here for the purpose.

The rotating disk problem was first investigated by von Karman [23] in 1921. He transformed the well-known Navier-Stokes equations into coupled ordinary differential equations using similarity transformations. After the work of von Karman, many of the researchers took interest in the study of rotating disk boundary-layers [24-27]. Bachok *et al.* [28] studied the effect of nanofluid on heat transfer in rotating flow near a porous disk. Turkyilmazoglu [29] considered the same flow for a non-porous disk taking five different types of nanoparticles. Enhanced heat transfer rates were noticed in both the studies [28, 29] where the uniform homogenous model of nanofluid was considered. Further results on rate of heat and mass transfer enhancement can be found in recent studies concerning rotating disk systems [30-32]. In all these studies [28-32] the nanoparticle concentration gradient as well as dependence of fluid properties on nanoparticle distribution have not been taken into account. This provides a room for studying heat and mass transfer enhancement in a rotating disk system using the idea of non-homogeneous distribution of nanoparticles in the boundary-layer. The objective of this article is to consider forced convection heat and mass transfer phenomena in a rotating disk boundary-layer. The fluid properties are considered as variable, depending upon the nanoparticle concentration. Enhanced rate of heat transfer has been calculated and the effects of nanoparticle concentration on mass-flow rate and moment coefficients are also highlighted. Results are interpreted through several graphs and tables.

Mathematical formulation

Nanofluid modeling

Consider a mixture of a pure fluid and metallic particles of nano size in it. The concentration of nanoparticles in the base fluid is fixed as ϕ_∞ (in percent). The presence of nanoparticles in the base fluid alters the material properties of the mixture such as viscosity, density and thermal conductivity. Because of the diverse nature of nanofluids with regrad to the nature, size, shape and concentration of the nanoparticle within the base fluid, it is quite hard to propose a

single model for every such property which would be applicable everywhere in general. So far, the theory and experiment have not been succeeded in doing so. Consequently, there exist several empirical and theoretical models for the description of effective viscosity, density and thermal heat capacity in the nanofluid. These models have their own merits and demerits with in the limited domain of applicability. For example, a list of several models, based on theory and experiment, for the effective viscosity of nanofluids is given in a nice book by Minkowytz *et al.* [33]. Most of the models have particularly been developed for nanoparticles of spherical shape. The spherical shaped nanoparticle with no intra interaction are usually preferred where the nanoparticles are required to behave, to some extent, as the fluid particles. Einstein [34] introduced the simplest model for effective viscosity of the nanofluid by using the hydrodynamic equations where the nanoparticle volume fraction was limited to 2% only in the form:

$$\mu = \left(1 + 2.5\phi\right)\mu_f \tag{1}$$

The Einstein's model (1) was further improved by Brinkman [35], Batchelor [36], and Lundgren [37] in order to extend it to high-moderate concentration or to incorporate the Brownian motion effects. Lundgren [37] simply assumed the Einstein's model as the first two terms of the Taylor series expansion of the form:

$$\mu = \frac{\mu_f}{1 - 2.5\phi} = \left(1 + 2.5\phi + 6.25\phi^2 + \ldots\right)\mu_f \tag{2}$$

and proposed the consideration of the complete series (2) instead of the first two terms. The model is however still limited to the dilute suspension of nanoparticles. The Batchelor's model [36] improves the Einstein's one by including a one more term of the Taylor series (2) whose coefficient is taken as 6.2 instead of 6.25 as in eq. (2). This model is actually based on the reciprocal theorem of Stokes flow and includes the effects of Brownian motion. The Brinkman model [35] also considers the Taylor series of the form:

$$\mu = \frac{\mu_f}{\left(1 - 2.5\phi\right)^{2/5}} \tag{3}$$

whose first two terms also cover the Einstein model. This model is applicable to the moderate and high concentration of the nanoparticle. In addition to these, there are several other nanofluid models for effective viscosity which are though limited to the spherical shaped nanoparticles but also include the radius of the spheres with some other restrictions. However literature is not limited to the spherical shaped nanoparticle but also includes some other shape such as cylinder, cone, brick, *etc.* Despite the presence of all such theoretical models the literature is also quite rich in the empirical models of the effective viscosity based wholly on the experimental data. Although, the empirical models are quite exact and have the capacity of predicting the very true results, but the problem with such models is that they are very limited in scope and apply only to those particular situations for which the corresponding experimental data have been collected. While in the theoretical analysis, as conducted in the current study, one is more inclined towards the general analysis of heat and mass transport phenomena in order to make a general qualitative analysis of the whole process. On this bases the theoretical models are usually being preferred having wider scope of applicability with some compromise on the qualitative measurements. Another aspect which is somehow more preferred by the theoretical analysits is the mathematical simplification of the chosen models. In the current analysis we choose to assume the spherical shape of nanoparticle and the moderate range for nanoparticle concentration. Ow-

ing to these properties and the mathematical ease the Brinkman model is observed to be the appropriate for current analysis.

The effective density of the nanofluid based on the physical rule of mixture is given:

$$\rho = (1-\phi)\rho_f + \phi\rho_p \tag{4}$$

which also shows an excellent agreement with the experiment. Maxwell [38] was the first to derive the effective thermal conductivity of the solid-liquid mixture and proposed that:

$$k = k_f\left[\frac{k_p + 2k_f + 2\phi\left(k_p - k_f\right)}{k_p + 2k_f - \phi\left(k_p - k_f\right)}\right] \tag{5}$$

which is applicable to the moderate concentration levels. The eq. (5) was extended to high concentration nanofluid by Bruggeman [39] in the form:

$$k = k_f\left[\frac{(3\phi-1)\frac{k_p}{k_f} + 3(1-\phi) - 1 + \sqrt{\Delta}}{4}\right] \quad \Delta = \left[\frac{(3\phi-1)k_p}{k_f} + 3(1-\phi) - 1\right]^2 + 8\frac{k_p}{k_f}$$

which readily reduces to the Maxwell's one for the case of moderate concentration. The thermal heat capacity of the nanofluid based on the analytical model reads:

$$\rho c = (1-\phi)(\rho c)_f + \phi(\rho c)_p \tag{6}$$

It has been shown in Minkowytz *et al.* [33] that the expansion eq. (6) finds an excellent agreement with the experimental data.

The Brownian motion diffusion coefficient and thermophoresis parameters are given:

$$D_B = \frac{k_B T}{3\pi\mu d_p}, \quad D_T = \beta\nu\phi \tag{7}$$

where the thermal expansion parameter β is defined:

$$\beta = (1-\phi)\beta_f + \phi\beta_p \tag{8}$$

An alternative definition of β is also available in literature with a certain modified form of the β given:

$$\rho\beta = (1-\phi)(\rho\beta)_f + \phi(\rho\beta)_p \tag{9}$$

In comparison to the experimental data both definitions of β do not find a good agreement; a poor approximation due to eqs. (8) and (9) can, however, not be denied. However, it has also been observed that the selection of eqs. (8) or (9) does not harm the results of skin friction and Nusselt number by any large. Staying on equal footing regarding the experimental data, eqs. (8) or (9) are equally valid with eq. (8) having an edge of mathematical simplicity.

Using the modified material parameters for nanofluid the conservation laws governing the convective transport phenomena are given:

$$\nabla(\rho\vec{\mathrm{v}}) = 0 \tag{10}$$

$$\rho\left[\frac{\partial\vec{\mathrm{v}}}{\partial t}+\left(\vec{\mathrm{v}}\nabla\right)\vec{\mathrm{v}}\right]=-\nabla p+\nabla\left[\mu\left(\nabla\vec{\mathrm{v}}+\nabla\vec{\mathrm{v}}^{T}-\frac{2}{3}\delta\nabla\vec{\mathrm{v}}\right)\right] \tag{11}$$

$$\rho\left[\frac{\partial h}{\partial t}+\left(\vec{\mathrm{v}}\nabla\right)h\right]=\nabla\left(k\nabla T\right)+\rho_p c_p\left(D_B\nabla\phi\nabla T+D_T\frac{\nabla T\nabla T}{T}\right) \tag{12}$$

$$\frac{\partial\phi}{\partial t}+\left(\vec{\mathrm{v}}\nabla\right)\phi=\nabla\left(D_B\nabla\phi+D_T\frac{\nabla T}{T}\right) \tag{13}$$

where $\vec{\mathrm{v}}=(v_r,v_\varphi,v_z)$ is the velocity vector, $h=cT$ – the enthalpy, $\nabla\vec{\mathrm{v}}$ – the velocity tensor gradient, and $\nabla\vec{\mathrm{v}}^{T}$ – the conjugate tensor gradient of velocity.

Governing equations

We consider a uniform flat disk of radius b resting at $z=0$ in 3-D space. The disk is surrounded by the homogeneous nanofluid. The radius of the disk is assumed to be large enough so that it is larger than the boundary-layer thickness; edge effects have been ignored due to which the flow resembles to that considered by von Karman for an infinite disk. The disk rotates about the z-axis with an angular speed ω. The disk temperature is fixed as T_w where the ambient temperature is assumed to be T_∞ such that $T_w<T_\infty$. A schematic of the flow geometry is shown in fig. 1.

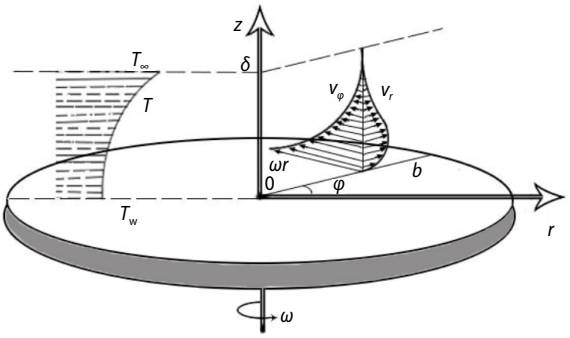

Figure 1. Schematic of the free rotating disk

The symmetry of the flow geometry requires consideration of cylindrical co-ordinates for further analysis. In this way the conservation laws, eqs. (10)-(13), readily read as in cylindrical co-ordinates:

$$\frac{1}{r}\frac{\partial\left(\rho r v_r\right)}{\partial r}+\frac{\partial\left(\rho v_z\right)}{\partial z}=0 \tag{14}$$

$$\rho\left(v_r\frac{\partial v_r}{\partial r}-\frac{v_\varphi^{\,2}}{r}+v_z\frac{\partial v_r}{\partial z}\right)=-\frac{\partial p}{\partial r}+\frac{\partial}{\partial r}\left[\frac{\mu}{r}\frac{\partial\left(rv_r\right)}{\partial r}\right]+\frac{\partial}{\partial z}\left(\mu\frac{\partial v_r}{\partial z}\right) \tag{15}$$

$$\rho\left(v_r\frac{\partial v_\varphi}{\partial r}+\frac{v_r v_\varphi}{r}+v_z\frac{\partial v_\varphi}{\partial z}\right)=\frac{\partial}{\partial r}\left[\frac{\mu}{r}\frac{\partial\left(rv_\varphi\right)}{\partial r}\right]+\frac{\partial}{\partial z}\left(\mu\frac{\partial v_\varphi}{\partial z}\right) \tag{16}$$

$$\rho\left(v_r\frac{\partial v_z}{\partial r}+v_z\frac{\partial v_z}{\partial z}\right)=-\frac{\partial p}{\partial z}+\frac{\partial}{\partial r}\left[\frac{\mu}{r}\frac{\partial\left(rv_z\right)}{\partial r}\right]+\frac{\partial}{\partial z}\left(\mu\frac{\partial v_z}{\partial z}\right) \tag{17}$$

$$\rho\left(v_r\frac{\partial h}{\partial r}+v_z\frac{\partial h}{\partial z}\right)=\frac{\partial}{\partial z}\left(k\frac{\partial T}{\partial z}\right)+\rho_p c_p\left[D_B\frac{\partial\phi}{\partial z}\frac{\partial T}{\partial z}+\frac{D_T}{T}\left(\frac{\partial T}{\partial z}\right)^2\right] \tag{18}$$

$$v_r \frac{\partial \phi}{\partial r} + v_z \frac{\partial \phi}{\partial z} = \frac{\partial}{\partial z}\left(D_B \frac{\partial \phi}{\partial z} + \frac{D_T}{T}\frac{\partial T}{\partial z} \right) \tag{19}$$

and the appropriate boundary conditions are:

$$\left.\begin{aligned} z = 0 : v_r = 0, \quad v_\varphi = r\omega, \quad v_z = 0, \quad T = T_w\left(h = h_w\right), \quad \left(D_B \frac{\partial \phi}{\partial z} \right)_{z=0} = -\left(\frac{D_T}{T}\frac{\partial T}{\partial z} \right)_{z=0} \\ z = \infty : v_r = 0, \quad v_\varphi = 0, \quad T = T_\infty\left(h = h_\infty\right), \quad \phi = \phi_\infty \end{aligned}\right\} \tag{20}$$

Self-similar solution

Due to its inherited nature, the von Karman swirling flow of a nanofluid on a rotating disk also admits separable solution of the form:

$$v_r = rf(z), \quad v_\varphi = rg(z), \quad v_z = h_v(z), \quad p = p(z), \quad h = h_E(z), \quad \phi = \phi(z) \tag{21}$$

The use of dimensional analysis under the implementation of Buckingham Pi theorem results in the new dimensionless variables:

$$\begin{gathered} \eta = z\sqrt{\frac{\omega}{\nu_f}}, \quad f = \omega F\left(\eta\right), \quad g = \omega G\left(\eta\right), \quad h_v = \sqrt{\nu_f \omega} H_v\left(\eta\right), \\ p = \rho_f \nu_f \omega P\left(\eta\right), \quad h_E = h_{E,\infty} H_E\left(\eta\right), \quad \phi = \Phi\left(\eta\right) \end{gathered} \tag{22}$$

The von Karman similarity transformations for velocity, pressure, enthalpy, and nanoparticles volume fraction are usually obtained as a combination of eqs. (21) and (22). Since the conventional notation for the dimensionless axial velocity in von Karman swirling flow is H which is also used as a conventional notation for dimensionless enthalpy function. In order to follow the use of conventional notation and to avoid any confusion, the subscripts v and E have been introduced. In this way h_v and H_v represent the velocity functions and h_E and H_E correspond to enthalpy functions in eqs. (21) and (22) and hence forth. The present formulation requires self-similar flow rates in order to establish the similarity solution. In doing so the variable nature of the density function is accommodated quite easily. Following Avramenko *et al.* [10] the self-similar flow rates are defined:

$$\rho v_r = \rho_\infty r\omega F\left(\eta\right), \quad \rho v_\varphi = \rho_\infty r\omega G\left(\eta\right), \quad \rho v_z = \rho_\infty \sqrt{\nu_f \omega} H_v\left(\eta\right) \tag{23}$$

where the ambient nanofulid density is used as the reference density. The functional dependence of thermophysical properties of nanofluid are described:

$$\rho = \rho(\phi), \quad \mu = \mu(\phi), \quad D_B = D_B(T), \quad D_T = D_T(\phi), \quad c = c(\phi), \quad k = k(\phi) \tag{24}$$

Utilizing eqs. (21)-(24) the conservation eqs. (14)-(19) immediately transform to the self-similar form:

$$H_v' + 2F = 0 \tag{25}$$

$$\begin{gathered} M\left[F'' - 2F'\Phi'\frac{R'}{R} + 2F\left(\Phi'\frac{R'}{R} \right)^2 - F\Phi'^2\frac{R''}{R} - F\Phi''\frac{R'}{R} \right] + \\ + \left(M'\Phi' - \overline{\rho} H_v \right)\left(F' - F\Phi'\frac{R'}{R} \right) - \overline{\rho}\left(F^2 - G^2 \right) = 0 \end{gathered} \tag{26}$$

$$M\left[G''-2G'\Phi'\frac{R'}{R}+2G\left(\Phi'\frac{R'}{R}\right)^2-G\Phi'^2\frac{R''}{R}-G\Phi''\frac{R'}{R}\right]+$$
$$+\left(M'\Phi'-\bar{\rho}H_v\right)\left(G'-G\Phi'\frac{R'}{R}\right)-2\bar{\rho}FG=0 \tag{27}$$

$$M\left[H_v''-2H_v'\Phi'\frac{R'}{R}+2H_v\left(\Phi'\frac{R'}{R}\right)^2-H_v\Phi'^2\frac{R''}{R}-H_v\Phi''\frac{R'}{R}\right]+$$
$$+\left(M'\Phi'-\bar{\rho}H_v\right)\left(H_v'-H_v\Phi'\frac{R'}{R}\right)-\frac{P'}{R}=0 \tag{28}$$

$$KH_E''+H_E'\left(\begin{array}{l}-\bar{\rho}\,\mathrm{Pr}H_v\dfrac{RC}{R}+\Phi'\left[K'+\dfrac{1}{\mathrm{Le}}+2\left(\dfrac{R'}{R}-\dfrac{RC'}{RC}\right)\left(K+\dfrac{\bar{D}}{\mathrm{Le}}\right)\right]+\\ +H_E\left\{\begin{array}{l}\left(\dfrac{R'}{R}-\dfrac{RC'}{RC}\right)\left[K\Phi''+\Phi'^2\left(\dfrac{1}{\mathrm{Le}}+K'\right)\right]+\Phi'^2\left[\bar{D}\left(\dfrac{R'}{R}-\dfrac{RC'}{RC}\right)^2+\right]+\\ +K\left(2\dfrac{RC'^2}{RC^2}-2\dfrac{R'}{R}\dfrac{RC'}{RC}+\dfrac{R''}{R}-\dfrac{RC''}{RC}\right)\end{array}\right\}\end{array}\right)$$
$$+\frac{\bar{D}}{\mathrm{Le}}\frac{H_E'^2}{H_E}=0 \tag{29}$$

$$\Phi''\left[1+\bar{D}\left(\frac{R'}{R}-\frac{RC'}{RC}\right)H_E\right]+\Phi'\left[\frac{H_E'}{D_B}\left(\frac{D_T'}{H_E}+D_B'\right)-\frac{\bar{\rho}}{R}\mathrm{Sc}H_v\right]+$$
$$+\Phi'^2\left[\left(\frac{R'}{R}-\frac{RC'}{RC}\right)\left(\frac{D_B'}{D_B}H_E+\frac{D_T'}{D_B}\right)+\bar{D}\left(\frac{RC'^2}{RC^2}-\frac{R'^2}{R^2}+\frac{R''}{R}-\frac{RC''}{RC}\right)\right]+\bar{D}\left(\frac{H_E''}{H_E}-\frac{H_E'^2}{H_E^2}\right)=0 \tag{30}$$

where

$$R(\Phi)=(1-\Phi)+\Phi\frac{\rho_p}{\rho_f},\quad RC(\Phi)=(1-\Phi)+\Phi\frac{\rho c_p}{\rho c_f},\quad M(\Phi)=(1-\Phi)^{-\frac{5}{2}},$$
$$K(\Phi)=\frac{k_p+2k_f+2\Phi(k_p-k_f)}{k_p+2k_f-\Phi(k_p-k_f)},\quad \mathrm{Pr}=\frac{\mu_f c_f}{k_f},\quad \mathrm{Sc}\left[H_E(\eta)\right]=\frac{\mu_f}{\rho_f D_B},$$
$$\bar{D}=\frac{D_T}{D_B},\quad \mathrm{Le}\left[H_E(\eta)\right]=\frac{\mathrm{Sc}\left[H^*(\eta)\right]}{\mathrm{Pr}}\frac{(\rho c)_f}{(\rho c)_p},\quad \bar{\rho}=\frac{\rho_\infty}{\rho_f} \tag{31}$$

Here the primes in the functions F, G, H_v, H_E, and Φ mean derivative with respect to η and primes in the function R, RC, M, K, and D_T mean derivative with respect to Φ and primes on D_B mean derivative with respect to H_E. From eq. (31) it is clear that the Prandtl number (as modeled) is independent of the influence of the nanoparticles. The boundary conditions (20) also transform to the self-similar form:

$$\eta = 0:\ F = 0,\quad G = \frac{R(\phi_{\mathrm{w}})}{\overline{\rho}},\quad H_v = 0,\quad P = 0,\quad H_E = \frac{h_{E,\mathrm{w}}}{h_{E,\infty}},\quad \frac{H_E}{H_E'} = \Phi'\left(\frac{RC'}{RC} - \overline{D}\right)$$
$$\eta = \infty:\ F = 0,\quad G = 0,\quad H_E = 1,\quad \Phi = \phi_\infty \tag{32}$$

where the subscripts w and ∞ with h_E denote the values of enthalpy at wall and ambient, respectively.

In order to accommodate the ratio $h_{E,\mathrm{w}}/h_{E,\infty}$ appearing in eq. (32), we replace enthalpy by temperature in energy eq. (18). In doing so, we also assume that specific heat capacity of the nanofluid is uniform c_∞ which is a valid assumption [10] and especially holds for large values of the Shmidt number, which is characteristic of flow of nanoparticle. Further D_B and D_T are also taken as constant, and constant temperature equal to T_∞ in the denominator of last term in eqs. (18) and (19). Under these assumptions eqs. (18) and (19) are must to be simplified to the following form:

$$K\theta'' + \theta'\left(\frac{\Phi'}{\mathrm{Le}} + K'\Phi' - \overline{\rho}\mathrm{Pr}H_v\right) + \frac{D}{\mathrm{Le}}\theta'^2 = 0 \tag{33}$$

$$\Phi'' - \frac{\overline{\rho}}{R}\mathrm{Sc}H_v\Phi' + D\theta'' = 0 \tag{34}$$

where

$$\theta(\eta) = \frac{T - T_{\mathrm{w}}}{T_\infty - T_{\mathrm{w}}},\quad \mathrm{Pr} = \frac{\mu_f c_\infty}{k_f},\quad \mathrm{Le} = \frac{\mathrm{Sc}}{\mathrm{Pr}}\frac{\rho_f}{\rho_p}\frac{c_\infty}{c_p},\quad D = \frac{T_\infty - T_{\mathrm{w}}}{T_\infty}\frac{D_T}{D_B}$$

Accordingly, the boundary data (32) also simplifies to:

$$\eta = 0: F = 0,\quad G = \frac{R(\phi_{\mathrm{w}})}{\overline{\rho}},\quad H_v = 0,\quad P = 0,\quad \theta = 0,\quad D\theta' + \Phi' = 0$$
$$\eta = \infty: F = 0,\quad G = 0,\quad \theta = 1,\quad \Phi = \phi_\infty \tag{35}$$

The analysis of current study strongly depends upon the role of some dimensionless physical parameters such as mass-flow rate, moment coefficient, displacement thickness, tangent of the flow swirl angle and the Nusselt number. The definitions of these parameters specific to the current study are given as the Nusselt number at the disk surface is defind by $\mathrm{Nu} = \alpha r/k_f$, where $\alpha = k(\partial T/\partial z)_{z=0}$. The moment coefficient on both sides of disk is given by $C_M = 2M/[(1/2)\rho_{\mathrm{nf}}\omega^2 b^5]$, where b is the radius of the disk (edge effects are ignored) and M is the moment defined as $M = -2\pi\int_0^b r^2\tau_{z\varphi}\mathrm{d}r$. The tangent of the flow swirl angle at the disk surface is calculated as [18] $\alpha_{\mathrm{w}} = -[(\partial v_r/\partial z)/(\partial v_\varphi/\partial z)]_{z=0}$, the mass-flow rate across the boundary-layer over the free rotating disk is calculated as $\dot{m}_d = 2\pi b\rho\int_{z=0}^{\infty} v_r\mathrm{d}z$, and the displacement thickness is defined:

$$\delta^* = \frac{1}{\omega r}\int_{z=0}^{\infty} v_\varphi \mathrm{d}z$$

Numerical solution

Numerical solution of the reduced boundary-layer eqs. (25)-(28), (33), and (34) corresponding to boundary data (35) is obtained through MATLAB built in software. Convergent

solution is obtained after several runs under the default tolerance level of 10^{-4}. The accuracy of the present numerical procedure is checked by solving the self-similar equations of pure fluid over a free rotating disk. A comparison of the present solution with that, already present in the literature [17] is given in tab. 1. The table shows an accurate match to four decimal places with the results obtained by Shevchuk [17] for different values of the Prandtl number. This authenticates the present solution procedure and allows for the solution of present equations using the same procedure.

Table 1. Comparison between present results and Shevchuk [17]

Pr	$\theta'(0)$		$F'(0)$		$G'(0)$	
	Shevchuk [17]	Present	Shevchuk [17]	Present	Shevchuk [17]	Present
0.10	0.0766	0.0766	0.5102	0.5102	–0.6159	–0.6159
1.00	0.3969	0.3969	0.5102	0.5102	–0.6159	–0.6159
10.0	1.1341	1.1341	0.5102	0.5102	–0.6159	–0.6159
13.0	1.2579	1.2579	0.5102	0.5102	–0.6159	–0.6159

Result and discussion

A detailed parametric analysis is made to understand the impact of nanofluid on heat transfer phenomena in rotating disk boundary-layer. Von Karman similarity variables are also shown to be applicable to the present model and a self-similar solution for varied values of the involved parameters, namely, Sc, ϕ_∞, D, and Pr is obtained. In most of the results ϕ_∞ is varied from 0.0 to 0.4 for Pr = 6 and strong convective heat transfer is observed. Values of Schmidt number Sc range from 10-100 in order to assume the base fluid as liquid. The diffusion parameter D is taken as 0.05 for most of the study. The presence of nanoparticles in the fluid also effects the momentum transport across the boundary-layer. The effect of Schmidt number on velocity components and pressure is shown in figs. 2 and 4.

Clearly, the influence of Sc is very weak on all the velocity components and slightly stronger on pressure. Pressure decreases within the boundary-layer by increasing the values of Sc. Similarly, the temperature profiles are not affected by changing the values of Sc parameter as shown in fig. 3. However strong dependence of the concentration profile on Sc can be seen in fig. 3. Clearly, concentration boundary-layer thickness decreases by increasing Sc number which reflects that the large values of Sc depreciate the mass transport phenomena across the boundary-layer and limit it to a very thin near-wall region. In comparison with momentum boundary-layer thickness, the concentration boundary-layer makes about 10% which means that over the most part of the momentum boundary-layer the nanoparticle concentration is uni-

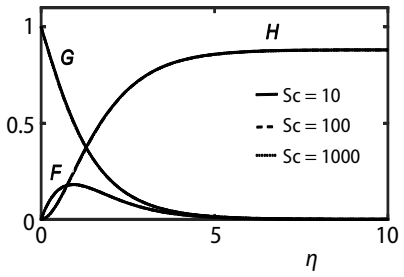

Figure 2. Radial, transverse, and axial components of velocity for different Sc at $\phi_\infty = 0.01$

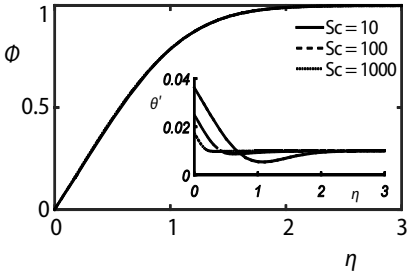

Figure 3. Temperature and concentration profile for different Sc at $\phi_\infty = 0.01$

form and is varying rapidly in the region close to the rotating disk. This is the reason that large values of Sc correspond to weak Brownian diffusion of nanoparticles. In such a situation nanofluid behaves more or less as a homogenous mixure. Therefore simulation of transport processes with a homogeneous mixture is justified for situations where Sc accepts large values. Figures 4 and 5 depict the effects of nanoparticle concentration ϕ_∞ on velocity components and pressure. It is clearly seen that all the velocity components are increased by increasing ϕ_∞.

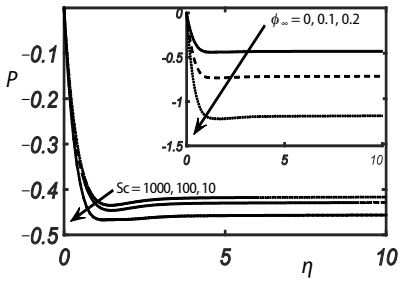

Figure 4. Effects of Sc (at $\phi_\infty = 0.01$) and ϕ_∞ at $(\mathrm{Sc} = 10)$ on pressure profile

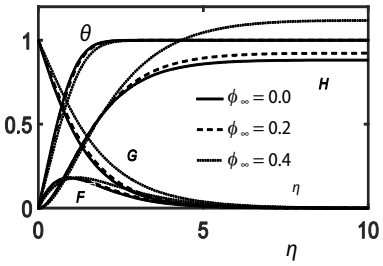

Figure 5. Radial, transverse and axial component of velocity and temperature profiles at Sc = 10

Furthermore, the boundary-layer thickness also increases by increasing the concentration level of nanoparticles. This mean that the presence of nanoparticles in the fluid enhances momentum transport across the boundary-layer. Figure 5 shows interesting impact of nanoparticles on the rotating disk boundary-layer. The downward axial velocity is enhanced by increasing the values of ϕ_∞. This, in turn, reflects the enhanced mass flux, which also favors heat transfer enhancement. This can immediately be confirmed from tab. 2 that the nanoparticle concentration enhances the relative mass-flow rate, and consequently the Nusselt number is also increased. Numerical values of the moment coefficient and the tangent of the flow swirl angle have also been reported in tab. 2 for varied values of nanoparticle concentration parameter ϕ_∞ and the Schmidt number. The results are very informative and quite impressive, highlighting the significance of non-homogeneous concentration profile of nanoparticles across the boundary-layer. The relative Nusselt number increases by increasing ϕ_∞ but decreases by increasing the Schmidt number for the fixed values of ϕ_∞. Furthermore, for small values of Schmidt number the rate of increase of $\mathrm{Nu}/\mathrm{Nu}_0$ with respect to ϕ_∞ is higher than that at large values of Schmidt number. This is because of the reason that at small Schmidt number values the non-homogeneous characteristic is somehow stronger and plays its role in heat transfer phenomena whereas at large values of Schmidt number, the concentration is treated as almost homogeneous in most part of the momentum boundary-layer. This fact highlights the importance of the present non-homogeneous model which correctly incorporates the contribution of nanoparticles towards momentum and thermal transport caused by their Brownian motion. In tab. 2, it is also shown that moment of the disk is highly influenced by nanoparticle concentration, meaning that the use of nanofluid in a rotating system increases its power as a consequence of enhanced moment. The effect of ϕ_∞ on the temperature profile is also shown in fig. 5. Analogous to the momentum boundary-layer the thermal boundary-layer also grows for increased values of ϕ_∞. Figures 6 and 7 depict the curves of the parameters $\mathrm{Nu}/\mathrm{Nu}_0$, C_m/C_{m0}, α_w/α_{w0}, and $\dot{m}_d/\dot{m}_{d0}$ against the nanoparticles concentration. Almost a linear relationship exists between ϕ_∞ and $\mathrm{Nu}/\mathrm{Nu}_0$ but non-linear for C_m/C_{m0}. The non-linearity becomes quite visible when the nanoparticle concentration becomes more than 20%, that is for $\phi_\infty > 0.2$. The tangent of the flow swirl angle α_w/α_{w0} does not depend upon the nanoparticle concentration, however, its value has been increased for nanofluid in comparison to base fluid.

Table 2. Relative values of important physical parameters when Pr = 6, $D = 0.05$, $\rho_p/\rho_f = 3.98195$

ϕ_∞	0	0.01	0.1	0.15	0.2	0.3	0.4
$Sc = 10(Nu/Nu_0)_{Le\to\infty}$	1	1.0537	1.3341	1.5001	1.6746	2.0528	2.4780
$(Nu/Nu_0)_{Le}$	1	1.0558	1.3368	1.5032	1.6781	2.0570	2.4828
C_m/C_{m0}	1	1.0418	1.3166	1.4925	1.6903	2.1744	2.8344
α_w/α_{w0}	1	1.0380	1.0356	1.0350	1.0348	1.0353	1.0369
$\dot{m}_d/\dot{m}_{d0}$	1	1.1084	1.3813	1.5569	1.7548	2.2417	2.9080
δ^*/δ_0^*	1	1.0060	1.0102	1.0284	1.0570	1.1481	1.2959
$Sc = 50(Nu/Nu_0)_{Le\to\infty}$	1	1.0391	1.3184	1.4839	1.6579	2.0350	2.4594
$(Nu/Nu_0)_{Le}$	1	1.0400	1.3196	1.4852	1.6593	2.0367	2.4614
C_m/C_{m0}	1	1.0329	1.3060	1.4809	1.6775	2.1586	2.8148
α_w/α_{w0}	1	1.0230	1.0215	1.0210	1.0207	1.0206	1.0209
$\dot{m}_d/\dot{m}_{d0}$	1	1.0836	1.3564	1.5317	1.7292	2.2139	2.8766
δ^*/δ_0^*	1	1.0025	1.0065	1.0242	1.0522	1.1420	1.2020
$Sc = 100(Nu/Nu_0)_{Le\to\infty}$	1	1.0355	1.3146	1.4800	1.6539	2.0311	2.4557
$(Nu/Nu_0)_{Le}$	1	1.0361	1.3153	1.4808	1.6548	2.0322	2.4570
C_m/C_{m0}	1	1.0308	1.3036	1.4781	1.6745	2.1550	2.8104
α_w/α_{w0}	1	1.0173	1.0162	1.0158	1.0155	1.0153	1.0153
$\dot{m}_d/\dot{m}_{d0}$	1	1.0740	1.3464	1.5212	1.7184	2.2016	2.8622
δ^*/δ_0^*	1	1.0014	1.0051	1.0226	1.0506	1.1400	1.2854
$Sc = 1000(Nu/Nu_0)_{Le\to\infty}$	1	1.0306	1.3097	1.4751	1.6491	2.0267	2.4522
$(Nu/Nu_0)_{Le}$	1	1.0307	1.3098	1.4753	1.6493	2.0269	2.4525
C_m/C_{m0}	1	1.0281	1.3003	1.4746	1.6706	2.1505	2.8050
α_w/α_{w0}	1	1.0054	1.0050	1.0047	1.0049	1.0046	1.0045
$\dot{m}_d/\dot{m}_{d0}$	1	1.0509	1.3234	1.4979	1.6948	2.1767	2.8343
δ^*/δ_0^*	1	0.9989	1.0024	1.0197	1.0474	1.1362	1.2807

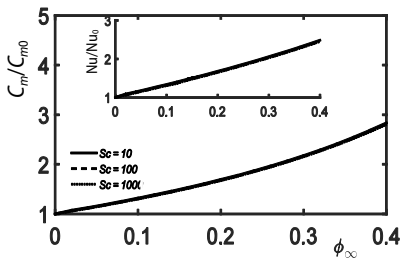

Figure 6. Relative moment coefficient and Nusselt number plotted against ϕ_∞

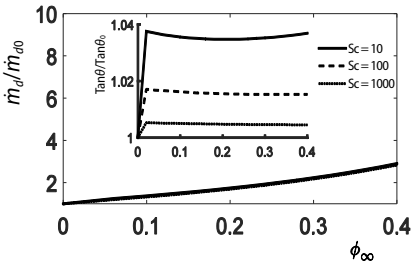

Figure 7. Relative mass-flow rate and tangent of the flow plotted against ϕ_∞

The relative mass-flow rate $\dot{m}_d/\dot{m}_{d0}$ for nanofluid also owns a non-linear relation with ϕ_∞ but the non-linearity weakens as ϕ_∞ grows. The quantative results of Nu/Nu_0, C_m/C_{m0}, α_w/α_{w0}, $\dot{m}_d/\dot{m}_{d0}$, and δ^*/δ_0^* are presented in tabs. 2-5 for specific values of Sc, D, Pr and ϕ_∞. Form tab. 2, it is noticed that the relative Nusselt number, the tangent of the flow swirl angle, moment coefficient, mass-flow rate, and displacement thickness are increased on increasing the nanoparticle concentration ϕ_∞. The values of all these parameters decrease by increasing the value of Schmidt num-

ber. The dependence of physical quantities of our interest such as Nusselt number, moment coefficient, tangent of angle of swirl, mass-flow rate, and the displacement thickness on the base fluid is an important aspect of this study. Present results help us to identify a particular base fluid that can be used in practical applications for optimal results. This analysis can be done from tabs. 3 and 4 where we have listed results for various values of the Prandtl number. Dependence of the Nusselt number upon Prandtl number is demonstrated through tab. 3 by giving percent increase in the rate of heat transfer. Clearly, at Sc = 10 the rate of heat transferis enhanced for fluids of large Prandtl numbers at $\phi_\infty = 0.01$ which is almost 128.51% when Prandtl number is increased from 0.1 to 13 (130 times). But for the nanofluid with 20% nanoparticles the enhancement is not that significant, which is almost 3.18%. Almost the same situation persists with some depreciation for Sc = 100. On the other hand the water with 20% nanoparticles gives almost a 68% increase in the rate of heat transfer in comparison to the pure fluid. This fact highlights the role of nanoparticles concentration towards heat transfer enhancement. Table 3 concludes that the Nusselt number is increased by considering the base fluid of large Prandtl number, but the major increase in the values of Nusselt number occurs at large concentration levels of nanoparticles. Relative values of the important physical parameters of current interest are listed in tab. 4 for different Prandtl numbers. From tab. 4 it is observed that, although the Nusselt number increases by increasing the Prandtl number, this increase is not significant. Similarly weak effects of Prandtl number are noted upon other parameters. It also reveals a weak dependence of above mentioned quantities on the Prandtl number, which means that a significant enhancement in the rate of heat transfer (as listed in tab. 3) is simply due to the presence of nanoparticles only and the nature of the base fluid does not matter considerably. However, at very low concentration levels, the fluids of large Prandtl number serve as a good coolant. In a similar fashion the role of

Table 3. Percent increase in the values of Nusselt number relative to the pure fluid calculated at different Pr when $D = 0.05$, $\rho_p/\rho_f = 3.98195$

Pr	Sc =10			Sc =100		
	$\phi_\infty = 0.01$	$\phi_\infty = 0.1$	$\phi_\infty = 0.2$	$\phi_\infty = 0.01$	$\phi_\infty = 0.1$	$\phi_\infty = 0.2$
0.1	2.8463%	30.2198%	66.5684%	2.8069%	30.1748%	66.5140%
1.0	3.7659%	31.5972%	66.3448%	3.0856%	30.8465%	65.5093%
6.0	5.5816%	33.6799%	67.8088%	3.6071%	31.5329%	65.4810%
10.0	6.1954%	34.3412%	68.3926%	3.8613%	31.8120%	65.6580%
13.0	6.5041%	34.6684%	68.6865%	4.0140%	31.9754%	65.7776%

Table 4. Relative values of important physical parameters for different values of Pr when $D = 0.05$, $\rho_p/\rho_f = 3.98195$, $\phi_\infty = 0.1$

Pr		0.1	1	6	10	13
Sc = 10	Nu/Nu_0	1.3022	1.3160	1.3368	1.3434	1.3467
	C_m/C_{m0}	1.3028	1.3122	1.3166	1.3162	1.3157
	α_w/α_{w0}	0.9922	1.0065	1.0237	1.0281	1.0030
	$\dot{m}_d/\dot{m}_{d0}$	1.3108	1.3439	1.3813	1.3919	1.3974
	δ^*/δ_0^*	1.0038	1.0122	1.0202	1.0219	1.0225
Sc = 80	Nu/Nu_0	1.3018	1.3088	1.3165	1.3197	1.3215
	C_m/C_{m0}	1.3004	1.3026	1.3042	1.3044	1.3044
	α_w/α_{w0}	0.9902	0.9969	1.0061	1.0090	1.0105
	$\dot{m}_d/\dot{m}_{d0}$	1.3066	1.3246	1.3497	1.3593	1.3640
	δ^*/δ_0^*	1.0022	1.0054	1.0097	1.0108	1.0113

diffusion parameter D has been demonstrated in tab. 5. It is calculated that an increase of almost 8%, 5%, 14%, 8%, and 7% occurs in the values of Nusselt number, moment coefficient, tangent of the flow swirl angle, displacement thickness, and mass-flow rate, respectively, when the values of D were increased by 20 times. It reveals an appreciable role of the diffusion parameter D towards flow and heat transfer enhancement. The discussion of tabs. 3-5 concludes that maximum gain in the rate of heat transfer is obtained by increasing the nanoparticle concentration and further enhancement is obtained by incorporating the role of nanoparticles diffusion within the boundary-layer and the nature of the base fluid does not affect largely.

Table 5. Effects of D for Pr = 6, ρ_p/ρ_f = 3.98195, ϕ_∞ = 0.1

D		0.01	0.05	0.1	0.15	0.2
Sc = 10	Nu/Nu_0	1.3145	1.3368	1.3640	1.3905	1.4163
	C_m/C_{m0}	1.3032	1.3166	1.3328	1.3483	1.3632
	α_w/α_{w0}	0.9955	1.0237	1.0598	1.0967	1.1347
	$\dot{m}_d/\dot{m}_{d0}$	1.3169	1.3809	1.4589	1.5348	1.6097
	δ^*/δ_0^*	1.0056	1.0202	1.0398	1.0592	1.0791
Sc = 80	Nu/Nu_0	1.3104	1.3165	1.3239	1.3310	1.3378
	C_m/C_{m0}	1.3007	1.3042	1.3086	1.3128	1.3168
	α_w/α_{w0}	0.9921	1.0061	1.0239	1.0418	1.0599
	$\dot{m}_d/\dot{m}_{d0}$	1.3110	1.3494	1.3960	1.4420	1.4871
	δ^*/δ_0^*	1.0031	1.0097	1.0180	1.0263	1.0348

Table 6 displays very important results regarding the non-homogeneous modeling of nanofluids which, of course, is the core issue highlighted in this communication. A comparison between the homogeneous (Tiwari and Das [5]) and non-homogeneous (Avramenko *et al.* [11]) models is made towards heat transfer enhancement. Computed values reflect that non-homogeneous model predicts increased rates of heat transfer, as compared to the homogeneous model at all concentration levels for all Prandtl numbers but the difference becomes wider when the nanoparticle concentration is 10% or higher. In particular, water with 20% nanoparticles produces almost 30% more gain in heat transfer rate for non-homogeneous model as compared to homogeneous model. This fact highlights the convection effects upon particles concentration within the boundary-layer which are usually ignored by the homogeneous models.

Table 6. Percent increase in heat transfer rate computed for homogeneous and non-homogeneous models

Pr	Homogeneous			Non-homogeneous (Sc = 10)		
	$\phi_\infty = 0.01$	$\phi_\infty = 0.1$	$\phi_\infty = 0.2$	$\phi_\infty = 0.01$	$\phi_\infty = 0.1$	$\phi_\infty = 0.2$
0.1	0.00%	0.94%	4.93%	2.85%	30.22%	66.57%
1.0	1.13 %	10.91%	22.03%	3.77%	31.60%	66.34%
6.0	1.60 %	15.85 %	31.83 %	5.58%	33.68%	67.81%
10.0	1.66%	16.53%	33.20%	6.19%	34.34%	68.39%
13.0	1.68%	16.80%	33.77%	6.50%	34.67%	68.69%

Conclusions

Self-similar solution for flow and heat transfer characteristics in a boundary-layer over a disk rotating in a nanofluid has been computed. The impact of nanoparticles is observed and calculated for various physical parameters of interest. The study reveals that the contribution of nanoparticles in the working fluid over a free rotating disk is manyfold. In addition to the pre-

sumed fact that the nanofluid enhances the rate of heat transfer, the rotating disk boundary-layer has benefited from the nanofluid in variety of ways. The flow and heat transfer phenomena of nanofluid basically depend upon the Schmidt number and the nanoparticle concentration ϕ_∞. Our analysis reveals that the role of Schmidt number in flow and heat transfer phenomena is not that significant but it strongly effects the concentration profile within the momentum boundary-layer. For large values of the Schmidt number the concentration layer becomes 10% of the momentum boundary-layer. However the variation in the values of ϕ_∞ contributes in different ways. The velocity profiles are enhanced due to the increased values of ϕ_∞ and stay unaltered by changing the Schmidt number. The pumping capacity of the disk is increased as a consequence of increased rate of mass-flow for nanofluid and the mass-flow rate further increases by increasing the nanoparticle concentration ϕ_∞. The presence of more nanoparticles in the nanofluid increases the moment coefficient of the disk. This fact indicates the advantage for the rotating system towards increased power when the working fluid is a nanofluid. The pressure falls for large the Schmidt number values whereas it grows in magnitude with the increase in concentration level of nanoparticles. The displacement thickness also increases with increased concentration.

Furthermore, it is also observed that the variation of Prandtl number for some fixed ϕ_∞ also gives augmentation towards heat transfer but it is not that significant as obtained by varying ϕ_∞ for any fixed Prandtl number. Overall 68% increase in the value of Nusselt number is observed when the base fluid is water with a 20% nanoparticle concentration. The comparison between homogeneous and non-homogeneous models reveals that the non-homogeneous model predicts further enhancement in heat transfer processes as compared to the homogeneous model. In this way the non-homogeneous model is observed to be more useful for studying the convection phenomena with nanofluids. A considerable increase (of almost 30%) in rate of heat transfer is computed through non-homogeneous modeling in comparison to homogeneous modeling when a mixture of water with 20% nanoparticles is used. This fact highlights the role of non-homogeneous concentration of nanoparticles within the boundary-layer.

References

[1] Maxwell, J. C., *Treatise on Electricity and Magnetism*, Oxford University Press, London, 1904
[2] Keblinski, P., *et al*., Mechanisms of Heat Flow in Suspensions of Nano-Sized Particles (Nanofluids), *International Journal of Heat and Mass Transfer*, *45* (2002), 4, pp. 855-863
[3] Choi, S. U. S., *Enhancing Thermal Conductivity of Fluids with Nanoparticle*, in: Developments and Applications of Non-Newtonian Flows, (Eds. D. A. Siginer, H. P. Wang), ASME, New York, USA, C, 231 (1995), 66, pp. 99-103
[4] Buongiorno, J., Convective Transport in Nanofluids, *Journal of Heat Transfer, 128* (2006), 3, pp. 240-250
[5] Tiwari, R. K., Das, M. K., Heat Transfer Augmentation in a Two-Sided Lid-Driven Differentially Heated Square Cavity Utilizing Nanofluids, *International Journal of Heat and Mass Transfer*, *50* (2007), 9-10, pp. 2002-2018
[6] Buschmann, M. H., Nanofluid in Thermosyphons and Heat Pipes: Overview of Recent Experiments and Modelling Approaches, *International Journal of Heat and Mass Transfer*, *52* (2009), Oct., pp. 3187-3196
[7] Rea, U., *et al*., Laminar Convective Heat Transfer and Viscous Pressure Loss of Alumina-Water and Zirconia-Water Nanofluids, *International Journal of Heat and Mass Transfer*, *52* (2009), 7-8, pp. 2042- 2048
[8] Magia, S. E. B., *et al*., Heat Transfer Behaviors of Nanofluids in Uniformly Heated Tube, *Supperlattices Microstructure, 35* (2004), 3-6, pp. 543-557
[9] Merhi, D., *et al*., Particle Migration in Concentrated Suspensions Flowing between Rotating Plates: Investigations of Diffusion Flux Coefficients, *Journal of Rheology, 49* (2005), 6, pp. 1429-1448
[10] Avramenko, A. A., *et al*., Self-Similar Analysis of Fluid Flow and Heat-Mass Transfer of Nanofluids in Boundary Layer, *Physics of Fluids, 23* (2011), 8, pp. 1-8
[11] Avramenko, A. A., *et al*., Symmetry Analysis and Self-Similar Forms of Fluid Flow and Heat-Mass Transfer in Turbulent Boundary Layer Flow of a Nanofluid, *Physics of Fluids, 24* (2012), 9, pp. 1-20
[12] Frank, M., *et al*., Particle Migration in Pressure Driven Flow of a Brownian Suspension, *Journal of Fluid Mechanics, 493* (2003), June, pp. 363-378

[13] Ding, Y. L., *et al.*, Particle Migration in a Flow of Nanoparticles Suspensions, *Powder Technology, 149* (2005), 2-3, pp. 84-92
[14] Avramenko, A. A., *et al*., Heat Transfer at Film Condensation of Stationary Vapor with Nanoparticles Near a Vertical Plate, *Applied Thermal Engineering, 73* (2014), 1, pp. 389-396
[15] Avramenko, A. A., *et al*., Heat Transfer at Film Condensation of Moving Vapor with Nanoparticles Near a Flat Surface, *International Journal of Heat and Mass Transfer*, *82* (2015), 1, pp. 316-324
[16] Avramenko, A. A., *et al*., Heat Transfer in Stable Film Boiling of Nanofluid over a Vertical Surface, *International Journal of Heat and Mass Transfer*, *92* (2015), June, pp. 106-118
[17] Shevchuk, I. V., *Convective Heat and Mass Transfer in Rotating Disk Systems*, Springer-Verlag, Berlin Heidelberg, 2009
[18] Lingwood, R. J., Absolute Instability of the Boundary Layer on a Rotating Disk, *Journal of Fluid Mechanics, 299* (1995), Sept., pp. 17-33
[19] Pier, B., Finite-Amplitude Crossflow Vortices, Secondary Instability and Transition in the Rotating-Disk Boundary Layer, *Journal of Fluid Mechanics, 487* (2003), June, pp. 315-343
[20] Carpenter, P. W., Thomas, P. J., Flow over a Compliant Rotating Disks, *Journal of Engineering Mathematics, 57* (2007), 3, pp. 303-315
[21] Davies, C., Carpenter, P. W., Global Behavior Corresponding to the Absolute Instability of the Rotating-Disk Boundary Layer, *Journal of Fluid Mechanics, 486* (2003), June, pp. 287-329
[22] Imayama, S., Experimental Study of the Rotating-Disk Boundary Layer Flow, Ph. D. thesis, Linne FLOW Centre, KTH Mechanics, Royal Institute of Technology SE-100 44 Stockholm, Sweden
[23] Karman, T. V., About Laminar and Turbulent Flow, *Z. Angew. Math. Mech., 1* (1921), Aug., pp. 233-252
[24] Cochran, W. G., The Flow Due to a Rotating Disk, *Mathematical Proceedings of the Cambridge Philosophical Society, 30* (1934), July, pp. 365-375
[25] Benton, E. R., On the Flow Due to a Rotating Disk, *Journal of Fluid Mechanics, 24* (1966), 4, pp. 781-800
[26] Mehmood, A., *et al*., Unsteady von Karman Swirling Flow: Analytic Study Using the Homotopy Method, *International Journal of Applied Mathematics and Mechanics, 6* (2010), 2, pp. 67-84
[27] Attia, H. A., Hassan, A. L. A., On Hydromagnetic Flow Due to a Rotating Disk, *Applied Mathematical Modelling, 28* (2004), 12, pp. 1007-1014
[28] Bachok, N., *et al*., Flow and Heat Transfer over a Rotating Porous Disk in Nanofluid, *Physica B, 406* (2011), 9, pp. 1767-1772
[29] Turkyilmazoglu, M., Nanofluid Flow and Heat Transfer Due to a Rotating Disk, *Comp. Phy., 94* (2014), May, pp. 139-146
[30] Rashidi, M. M., *et al*., Entropy Generation in Steady MHD Flow Due to a Rotating Porous Disk in a Nanofluid, *International Journal of Heat and Mass Transfer*, *62* (2013), July, pp. 515-525
[31] Yin, C., *et al*., Flow and Heat Transfer of Nanofluids over a Rotating Porous Disk with Velocity Slip and Temperature Jump, *Z. Naturforsch. A, 70* (2015), 5, pp. 351-358
[32] Liu, I. C., *et al*., Flow and Heat Transfer of Nanofluids Near a Rotating Disk, *Advanced Martial Research, 664* (2013), Feb., pp. 859-865
[33] Minkowycz, W. J., *et al.*, *Nanoparticles Heat Transfer and Fluid Flow*, CRC Press, Taylor and Franics Group, Boca Raton, London, New York, 2013
[34] Einstein, A., Eine neue bestimmung der molekuldimensionen, *Annalen der Physik, Leipzig, 19* (1906), pp. 289-306
[35] Brikmann, H. C., The Viscosity of Concentrated Suspensions and Solutions, *Journal of Chemical Physics, 20* (1952), 4, pp. 571-581
[36] Batchelor, G., The Effect of Brownian Motion on the Bulk Stress in a Suspension of Spherical Particles, *Journal of Fluid Mechanics, 83* (1977), 1, pp. 97-117
[37] Lundgren, T., Slow Flow through Stationary Random Beds and Suspension of Spheres, *Journal of Fluid Mechanics, 51* (1972), 2, pp. 273-299
[38] Maxwell, J. C. A., *Treatise on Electricity and Magnetism*, Calrendon Press, Oxford, UK, 2nd ed., 1881
[39] Brugeman, D. A. G., Berechnung verschiedener physikalischer konstanten von hetrogenen substanzen, I. Dielektrizitatskonstanten und lietfahigkiten der mischkorper aus isotropen substanzen, *Annaln der Physik*, Leipzig, *24* (1935), pp. 636-679

Paper submitted: April 12, 2016
Paper revised: November 5, 2016
Paper accepted: November 9, 2016